Role for Pro-13 in Directing High-Affinity Binding of Anthopleurin B to the Voltage-Sensitive Sodium Channel†

Gregory J. Kelso,‡ Chester L. Drum,§ Dorothy A. Hanck,§ and Kenneth M. Blumenthal*,‡

Department of Molecular Genetics, Biochemistry and Microbiology, University of Cincinnati College of Medicine, Cincinnati, Ohio 45267, and the Departments of Medicine and Pharmacological and Physiological Sciences, University of Chicago, Chicago, Illinois 60637

Received July 1, 1996; Revised Manuscript Received September 16, 1996⊗

ABSTRACT: Anthopleurin A (ApA) and B (ApB) are 49-amino acid polypeptide toxins from the Pacific sea anemone *Anthopleura xanthogrammica* that interfere with inactivation of voltage-gated sodium channels. ApA, which differs from ApB in seven of the 49 amino acids, displays markedly enhanced isoform selectivity compared with ApB, acting preferentially on cardiac over neuronal sodium channels. Previous studies in this lab have indicated the importance of two unique charged residues in ApB, Arg-12 and Lys-49, in this toxin's ability to discriminate between neuronal and cardiac sodium channels. Likewise, a double mutant (R12S/K49Q) recently characterized in this lab (Khera et al., 1995) displays a greatly reduced affinity for neuronal channels, essentially restoring the discriminatory ability of ApA. When the remaining five residues unique to ApB are individually converted to those of ApA, only ApB (Pro-13) shows a major effect, reducing the affinity of the new mutant toxin (P13V) against both channel isoforms approximately 10-fold. This effect is most likely the result of a conformational rearrangement within the surrounding cationic cluster which includes Arg-12 and -14, as well as Lys-49. However, when placed into the context of the double mutant R12S/K49Q a unique effect is observed: the new triple mutant (R12S/P13V/K49Q) is no longer able to discriminate effectively between channel isoforms. Its affinity for the neuronal sodium channel is significantly *enhanced* compared to either P13V or to the double mutant R12S/K49Q. These results are consistent both with our proposed model (Khera et al., 1995) and with the recently reported solution structure of ApB, which implicate the cationic cluster in both affinity and channel isoform selectivity. We suggest that the P13V mutation results in a shift in the relative orientation of cationic residues within the large flexible loop between residues 9−18, thus strengthening their interactions with target sequences of the neuronal sodium channel.

Significant progress has been made in elucidating the structural basis underlying the functional properties of the voltage-dependent sodium channel [reviewed in Catterall (1995) and Fozzard and Hanck (1996)]. The development of a molecular map of the sodium channel whose framework originated in determination of its deduced primary structure (Noda et al., 1984) has evolved through the concerted effort of many laboratories worldwide. A variety of neurotoxins have been useful tools for study of the sodium channel, and they can be classified into two broad groups: blockers and modulators (Narahashi & Herman, 1992). Included among the modulators are a group of polypeptide toxins isolated from anemone and scorpion venoms, which have been classified as site 3 toxins by Catterall (1984). They bind at a common extracellular site (Ray et al., 1978) and interfere with sodium channel inactivation from the open state without affecting activation kinetics or inactivation from closed states (Hanck & Sheets, 1995). A portion of the binding site for the α-scorpion toxins has been localized to the extracellular loop between transmembrane helices S5 and S6 of domains I and IV of the sodium channel α-subunit (Tejedor & Catterall, 1988), and competition binding studies with sea anemone toxins indicate that both classes of toxins share the same binding site (Catterall & Beress, 1978).

Anemone toxins isolated from *Anthopleura xanthogrammica*, anthopleurin A (ApA) and B (ApB), are attractive probes of sodium channel structure because of their high affinity and ability to discriminate effectively between the neuronal and cardiac channel isoforms (Schweitz et al., 1981; Kem et al., 1989). They are members of a family of small (4000−6000 Da), basic polypeptides which act primarily on fast sodium channels. The action of anemone toxins has been studied with a variety of assays. In murine neuroblastoma cells, ApB is an effective enhancer of veratridine-dependent, TTX-sensitive Na^+ uptake, with an ED_{50} of 7 nM (Schweitz et al., 1981). Whole animal studies, as well as analysis in isolated heart preparations, show ApA exerts a positive inotropic action on the heart, with EC_{50} values ranging from 1 to 3 nM for a variety of mammalian heart tissues (Shibata et al., 1976; Alsen et al., 1976; Ravens, 1976). More recently, ApA was studied in ischemic dog hearts, where its intravenous administration (1.5−5.0 mg/kg) sustains a positive inotropic effect after 30 min with no evidence for deterioration of function or arrhythmias (Gross

† This research was supported by Grant HL-41543 from the National Institutes of Health (K.M.B.) and HL-P01-20592 (D.A.H.). D.A.H. is an Established Investigator of the American Heart Association.

* Address correspondence to this author at University of Cincinnati College of Medicine, Department of Molecular Genetics, Biochemistry and Microbiology, 231 Bethesda Avenue, Cincinnati, OH 45267-0524. Phone: (513) 558-5505. Fax: (513) 558-8467. E-mail: BLUMENKM@uc.edu.

‡ University of Cincinnati College of Medicine.

§ University of Chicago.

⊗ Abstract published in *Advance ACS Abstracts,* November 1, 1996.

S0006-2960(96)01584-X CCC: $12.00

et al., 1985). Because anemone toxins are known to have a positive inotropic effect in isolated cardiac preparations as well as whole animals, their potential as cardiotonic agents clearly exists.

ApB has long been recognized to have the highest affinity of all known anemone toxins for mammalian sodium channels (Schweitz et al., 1981). The closely related isoform, ApA, shares a high affinity for the cardiac sodium channel (14 nM) while exhibiting a 30-fold lower affinity for the neuronal isoform (400 nM) by ion flux assay (Gallagher & Blumenthal, 1994). Interestingly, when affinity is assayed by voltage clamp not only do neuronal channels differentiate between ApA and ApB (120 nM vs 5.1 nM) but cardiac sodium channels also differentiate (2.5 nM vs 0.1 nM) (Khera et al., 1995). Because ApA could potentially yield novel insights into toxin determinants involved in isoform discrimination, a stepwise substitution of ApB to ApA has been undertaken to identify the subset of residues responsible. As depicted below, ApB differs from ApA at seven positions (in boldface type).

ApA: GV**S**CLCDSDGP**SV**RGNTLSG**T**LW**L**YPSGCPSGWHNCKAHGP**T**IGWCCK**Q**

ApB: GV**P**CLCDSDGP**RP**RGNTLSG**I**LW**F**YPSGCPSGWHNCKAHGP**N**IGWCCK**K**

Previous studies in this lab indicated the importance of two unique cationic residues in ApB, Arg-12 and Lys-49, in affecting the toxin's ability to discriminate between neuronal and cardiac sodium channels (Gallagher & Blumenthal, 1994). Most recently, we showed that simultaneous mutation of both sites (R12S/K49Q), reduces the affinity of the mutant for neuronal channels to a much greater extent than the cardiac counterparts, essentially restoring the discriminatory ability inherent in ApA (Khera et al., 1995).

In the present study, we have used site-directed mutagenesis to target the remaining five residues which differ between ApB and ApA. Each was mutated individually and a new triple mutant (R12S/P13V/K49Q) was constructed. The functional contributions of these substitutions were assessed by measuring their ability to enhance veratridine-dependent, TTX-sensitive $^{22}Na^+$ uptake in both cultured cardiac and neuroblastoma cells. In addition, the triple mutant (R12S/P13V/K49Q) was evaluated electrophysiologically. Of the five individual sites characterized, only Pro-13 showed a major effect, reducing the affinity of the new mutant toxin (P13V) toward both sodium channel isoforms approximately 10-fold. However, when combined with the double mutant (R12S/K49Q), a unique effect is observed. The new triple mutant, (R12S/P13V/K49Q) loses the ability to discriminate normally between sodium channel isoforms, displaying a 2-fold increase in apparent affinity over the P13V single mutant for the neuronal isoform. These results are interpreted within the context of our proposed model, implicating the cluster of basic residues including Arg-12, Arg-14, Lys-48, and Lys-49 in both affinity and channel isoform selectivity (Khera et al., 1995).

EXPERIMENTAL PROCEDURES

Materials. Restriction enzymes, T4 DNA ligase, and Taq DNA polymerase were purchased from Gibco/Bethesda Research Laboratories. DNase, RNase, leupeptin, pepstatin, phenylmethylsulfonyl fluoride (PMSF), ouabain, and veratridine were obtained from Sigma. Deoxynucleotide triphosphates (dNTP's) used in the polymerase chain reaction were purchased from Pharmacia LKB Biotechnology Inc., and staphylococcal protease (V8 protease) was from ICN. Chicken lysozyme, isopropyl 1-thio-β-D-galactopyranoside (IPTG), and the Sequenase Version 2.0 sequencing kit were obtained from U.S. Biochemical Corp. ^{22}NaCl and ^{32}P-dATP were purchased from Dupont NEN. Dulbecco's Modified Eagle's Medium (DMEM) was obtained from both JRH Biosciences and Mediatech. Fetal calf serum was purchased from both United Biochemical Inc. and Hyclone Laboratories. C_4 semi-preparative and analytical HPLC columns were purchased from SynChrom Inc. Other chemicals and reagents were analytical grade products of Sigma or Fisher.

Cell Culture. The murine neuroblastoma cells (N1E-115) were provided by Dr. Marshall Nirenberg (National Heart, Lung, and Blood Institute, NIH), and the rat tumor cell line RT4-B was provided by Dr. Laurie Donahue (Health Sciences Center, Texas Tech University). The N1E-115 line has been shown to express the rat brain type II sodium channel by PCR analysis (Hirsh & Quandt, 1996), while RT4-B cells express the cardiac/denervated skeletal muscle isoform (Donahue et al., 1991; Zeng et al., 1996). Sodium currents in these lines display the expected TTX-sensitivities. N1E-115 cells were grown in DMEM (JRH Biosciences) supplemented with 10% heat-inactivated fetal calf serum (Hyclone Laboratories) containing 110 units/mL each of penicillin and streptomycin, while the RT4-B cells were grown in DMEM (Mediatech) supplemented with 10% fetal calf serum (United Biochemical, Inc.) also containing 110 units/mL each of penicillin and streptomycin. All cells were maintained at 37 °C in a humidified incubator with 10% CO_2 in 75 cm^2 tissue culture flasks. For passage, cells were harvested with either 0.25% trypsin (RT4-B) or 10 mM NaH_2PO_4, 150 mM NaCl, 3 mM KCl, 3 mM KH_2PO_4, pH 7.4 (N1E-115), and reseeded at a density of 1×10^6 per flask or 5×10^4 per well in 24-well plates for sodium uptake assays. After attaining confluency, N1E-115 cells were maintained an additional 48 h in differentiation media consisting of DMEM containing 1.5% heat-inactivated fetal calf serum, 1.5% dimethyl sulfoxide, and 110 units/mL each of penicillin and streptomycin prior to use in the sodium uptake assays to enhance cell adherence.

Site-Directed Mutagenesis of Recombinant ApB. All of the mutants described here were constructed by site-directed mutagenesis via the polymerase chain reaction. The expression vector pKB-13 (Khera et al., 1995) containing a synthetic ApB gene was used as a template. Appropriate primers containing the mutation of interest (Table 1) were synthesized and annealed to the ApB template for 30 rounds of PCR. Correctly sized PCR product was then ligated to the ApB plasmid following digestion by appropriate restriction enzymes. All ApB mutants were verified prior to protein expression by double-stranded dideoxy sequencing (Sanger et al., 1977) using the Sequenase protocol. The *Escherichia coli* strain DH5a was used for plasmid propagation.

Protein Expression. Plasmid containing the desired mutation was transformed into *E. coli* strain BL-21(DE3) for expression of high levels of toxin fusion protein as previously described (Gallagher & Blumenthal, 1992). This host strain contains a copy of the T7 RNA polymerase gene under control of a lac UV5 promoter, permitting IPTG-inducible expression of the fusion protein. After expression, the soluble fusion protein was purified by anion exchange chromatography and then treated with a glutathione redox

Table 1: Amino Acid Compositions of Recombinant *Anthopleura* Toxins[a]

amino acid	ApB	P13V	P3S	I21T	N42T	F24L	R12S P13V K49Q
Asx	4.7(5)	5.5(5)	5.0(5)	4.7(5)	**4.2(4)**	5.2(5)	4.8(5)
Glx	0.6(0)	1.1(0)	1.1(0)	0.2(0)	1.4(0)	0.6(0)	**1.8(1)**
Ser[b]	3.6(4)	4.7(4)	**4.5(5)**	3.6(4)	3.5(4)	4.0(4)	**4.4(5)**
Gly	8.0(8)	7.0(8)	8.1(8)	7.6(8)	7.0(8)	8.0(8)	7.8(8)
His	1.7(2)	1.7(2)	1.7(2)	1.9(2)	1.9(2)	1.7(2)	1.8(2)
Arg	2.1(2)	2.6(2)	2.0(2)	1.9(2)	2.1(2)	2.1(2)	**1.1(1)**
Thr	1.3(1)	1.5(1)	1.2(1)	**1.9(2)**	**2.1(2)**	1.1(1)	1.0(1)
Ala	1.4(1)	1.3(1)	1.3(1)	1.2(1)	1.4(1)	1.1(1)	1.0(1)
Pro	5.9(6)	**5.3(5)**	**5.3(5)**	5.6(6)	6.1(6)	6.4(6)	**5.4(5)**
Tyr	0.9(1)	1.3(1)	1.0(1)	1.0(1)	1.0(1)	0.7(1)	1.0(1)
Val	1.4(1)	**1.7(2)**	1.2(1)	1.0(1)	1.2(1)	1.1(1)	**1.9(2)**
Met	0.1(0)	0.7(1)	0.2(0)	0.1(0)	0.1(0)	0.0(0)	0.1(0)
Cys	nd[c]	nd	nd	nd	nd	nd	nd
Ile	2.3(2)	1.8(2)	2.0(2)	**1.1(1)**	2.2(2)	1.9(2)	2.3(2)
Leu	3.2(3)	2.8(3)	3.0(3)	3.2(3)	3.2(3)	**4.0(4)**	2.8(3)
Phe	1.3(1)	1.0(1)	1.1(1)	0.9(1)	1.2(1)	**0.0(0)**	1.0(1)
Trp	nd	nd	nd	nd	nd	nd	nd
Lys	2.9(3)	2.3(3)	2.6(3)	(3)	3.0(3)	2.9(3)	**2.1(2)**
MW[d]	5260 (5388)	nd	5255 (5385)	5241 (5369)	5250 (5380)	5228 (5355)	5205 (5332)
MW[e]	5275 (5403)	5277	5265 (5393)	5263 (5391)	5260 (5388)	5224 (5352)	5209 (5337)

[a] Theoretical values are shown in parentheses, and residue numbers differing from those in wild-type ApB are presented in boldface type. [b] Values for serine and threonine are not corrected for partial destruction during acid hydrolyis, and values for valine and isoleucine are uncorrected for incomplete hydrolysis after 24 h. [c] nd, not determined. [d] Determined by MALDI-TOF mass spectrometry. The minor *m*/*z* form, where present, is in parentheses. [e] Calculated by summation of the known amino acid sequence.

couple containing 1 mM GSH and 0.2 mM GSSG to allow oxidation of the toxin's three disulfide bonds. Ultimately, the ApB mutant was liberated from the fusion protein using V8 protease and purified to homogeneity by reverse-phase HPLC.

Amino Acid Analysis. Samples were hydrolyzed in the presence of 6 M HCl *in vacuo* and derivatized with phenyl isothiocyanate. Following derivatization, amino acid compositions were determined with the Waters PICO-TAG system. Amino acid analyses were performed by the Protein Chemistry Facilities in the Department of Pharmacology and Cell Biophysics, University of Cincinnati College of Medicine, or the Department of Biochemistry, University of Louisville Medical College. Molecular weights were determined by MALDI-TOF mass spectrometry of HPLC-purified samples.

Circular Dichroism. Circular dichroic (CD) spectra for all ApB mutants were obtained on a Jasco 710 spectropolarimeter calibrated with d_{10}-camphorsulfonic acid. Protein secondary structure was estimated by comparison to a database containing proteins of known structure (cytochrome *C*, ribonuclease A, myoglobin, hemoglobin, papain, α-chymotrypsin, trypsin, lysozyme, and alcohol dehydrogenase), using the least-squares method (Protein Secondary Structure Estimation Program, Japan Spectroscopic Co. Ltd.).

Sodium Uptake Assay. Sodium uptake was measured according to well-established protocols utilized in this laboratory (Gallagher & Blumenthal, 1994). Briefly, cells expressing either neuronal (N1E-115) or cardiac (RT4-B) forms of the sodium channel were preincubated at 37 °C for 30 min in sodium-free buffer containing 20 mM veratridine and increasing concentrations of toxin. Uptake was initiated by replacing this medium with one containing toxin and 5 mM ^{22}NaCl (1 mCi/mL) and terminated after 60 s by washing with ice-cold Na^+-free buffer. Cells were solubilized, and total protein was determined by the method of Bradford (1976). V_{max} and $K_{0.5}$ were calculated by fitting the data to a single hyperbolic function according to Cleland (1979) after correcting for veratridine-dependent uptake. The calculated values are based on data from between four and 16 individual uptake experiments.

Electrophysiological Methods. *(a) Preparation and Solutions*. RT4-B cells were isolated from culture dishes using 0.25% trypsin with 1 mM EDTA-4Na in HBSS (#25200, Gibco BRL, Gaithersburg, MD). The N1E-115 cells were mechanically separated from dishes. Both cell types were then centrifuged, and the pellet was suspended in bath solution, where it was stored until transfer to the recording chamber.

For both cell types, the control bath solution consisted of 70 mM NaCl, 70 mM CsCl, 1 mM $CaCl_2$, 1 mM $MgCl_2$, and 10 mM HEPES, pH 7.4. The pipet solution contained 130 mM CsF, 10 mM CsCl, and 10 mM HEPES, pH 7.4. All toxin solutions were made of the bath solution, 0.5% bovine serum albumin (BSA), and the specified concentration of toxin. Toxin recording solutions were made 30 min prior to the beginning of each experimental day from flash-frozen aliquots stored in 0.5% BSA with 5 mM succinate, pH 4, and renewed approximately every 4 h.

(b) Recording Protocol. Recordings were made using an Axopatch 200 amplifier (Axon Instruments, Foster City, CA). Voltage protocols were executed on a 486DX2-50 computer running CLAMPEX 6.0.1 (Axon). Data were filtered at 5 kHz with a 4-pole Bessel filter and digitized at 50 kHz (12-bit resolution). Pipet resistances ranged from 700 kΩ to 1.1 MΩ. Suction was used to gain electrical access to the cell, and the cell was then voltage clamped to −140 mV (RT4-B) or to −120 mV (N1E-115). A current−voltage relationship was recorded, and a steady-state inactivation protocol was performed. In every case, the holding potential used was sufficiently hyperpolarized to assure complete availability of I_{Na}. Voltage control was determined by examination of the time to peak of the whole-cell current and the slope of the conductance transform. In order to measure

the time course of modification, cells were depolarized for 10 ms every 1 or 2 s (depending on the rate of modification). Separate current voltage and steady state inactivation protocols were taken after the modification in order to monitor continued voltage control. In order to observe dissociation of the toxin, 10 ms depolarizations were begun again at a rate of 1 or 0.5 Hz, and the cell was moved back to the control bath.

(c) Analysis. Modified current was taken as the average of the current between 7.6 and 8 ms, since for both channel isoforms all the unmodified current had decayed before this window. The averages were plotted against time and a single exponential curve fit to the data using a least-squares minimization routine included with the Origin 3.5.2 software (Microcal Software, Northampton, MA). In fitting, the first two points of a 1 Hz record train or the first point of a 0.5 Hz record train were excluded. Unmodification time constants were determined similarly. Because unmodification (toxin dissociation) is a first-order process, k_{off} was simply the inverse of the unmodification time constant. The on-rate (k_{on}) was determined through the relationship

$$k_{on} = \frac{(k_{mod} - k_{off})}{[T]}$$

where k_{mod} was the inverse of the fitted τ of modification time course and [T] the toxin concentration.

RESULTS

Expression and Purification of ApB Mutants. The *E. coli* strain BL21(DE3) which has been transformed with a plasmid containing the mutant ApB gene of choice produces in all cases similar amounts of fusion protein as obtained previously from both wild-type recombinant ApB and site-directed mutants (Gallagher & Blumenthal, 1992, 1994; Khera & Blumenthal, 1994; Khera et al., 1995). When the fusion protein is reoxidized and then digested with V8 protease, followed by HPLC purification, typical yields of 0.7−2.0 mg of toxin/g of fusion protein are routinely obtained. Comparison of the HPLC elution profiles (data not shown) shows similar retention times as compared to wild-type recombinant ApB, consistent with full oxidation of all disulfide bonds, although those mutants with an increase in hydrophobic character display slightly longer retention times.

Structural Characterization of ApB and ApB Mutants. Amino acid compositions for all of the ApB mutants constructed are presented in Table 1. With the exception that glutamic acid levels are elevated in most of the samples, the results are in each case consistent with those expected for the designed mutation. This glutamic acid artifact is most likely the result of incomplete protease cleavage of the fusion protein within the pentaglutamyl linker region N-terminal to the ApB sequence, resulting in a one-residue extension at the N-terminus. Recent sequencing and MALDI-TOF analysis (Table 1) confirm this hypothesis. As indicated in Table 1, each sample exhibiting elevated glutamate levels upon amino acid analysis also contained a major *m*/*z* peak corresponding to the normal, 49-residue form of ApB, and a minor form with a molecular mass greater by 128, precisely the contribution of a glutamate residue. As we have previously demonstrated that a different N-terminally extended ApB mutant, GR-ApB, has an activity identical to that of natural ApB (Gallagher & Blumenthal, 1992), we felt it unlikely that this additional glutamate would have a significant effect on activity. In order to test this possibility, the 49-residue forms of the P13V and R12S/P13V/K49Q mutants were purified by C_{18} HPLC in the presence of 4.6 mM HFBA. For these proteins, this protocol allowed base line separation of the extended and 49-residue forms of the toxins. Subsequent analysis of the latter by ion flux assay reveals them to be identical in both affinity and V_{max} of uptake to the mixtures from which they were derived (data not shown).

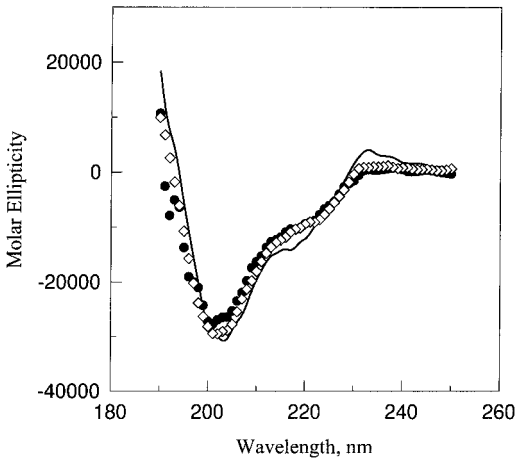

FIGURE 1: Far-UV circular dichroism spectra of ApB (solid line), P13V (diamonds), and R12S/P13V/K49Q (filled circles). Spectra were recorded at room temperature in 1.5 mM sodium phosphate buffer, pH 7.0, as described in Experimental Procedures.

In order to eliminate the possibility that mutationally-induced changes in activity merely reflect large-scale conformational rearrangements, CD spectra over the range of 190−250 nm were collected for all of the ApB mutants described here (Figure 1). These spectra are indistinguishable from those of wild-type ApB. Calculation of secondary structures indicates that all the mutant proteins display a primarily β-sheet conformation, in the range of 55−60%, with little or no α-helix. We also estimated the thermal stability of each of these proteins by collecting CD spectra in the presence of either 1.5 M Gdn-HCl or 4 M Urea, over the temperature range 24−80 °C. Secondary structure estimations derived from these spectra indicate that all toxins retain their full secondary structure throughout this temperature range (data not shown), again consistent with full oxidation of all disulfide bonds. Therefore, we are able to rule out large-scale conformationally-induced changes in activity when evaluating the effects of mutations to the ApB toxin.

Functional Characterization of ApB Mutants by Ion Flux. In order to ascertain the functional effects of mutating ApB, veratridine-dependent sodium uptake was measured in cultured murine neuroblastoma cells (N1E-115) and in rat tumor cells (RT4-B) as described in Experimental Procedures. Dose-response curves were generated for all ApB mutants characterized in this study, and a representative plot for the P13V mutant is shown in Figure 2. The kinetic constants $K_{0.5}$ and V_{max}, calculated as described in the Experimental Procedures, are listed in Table 2, and comparisons of $K_{0.5}$ values for all the mutants in this study are presented in Figure 3.

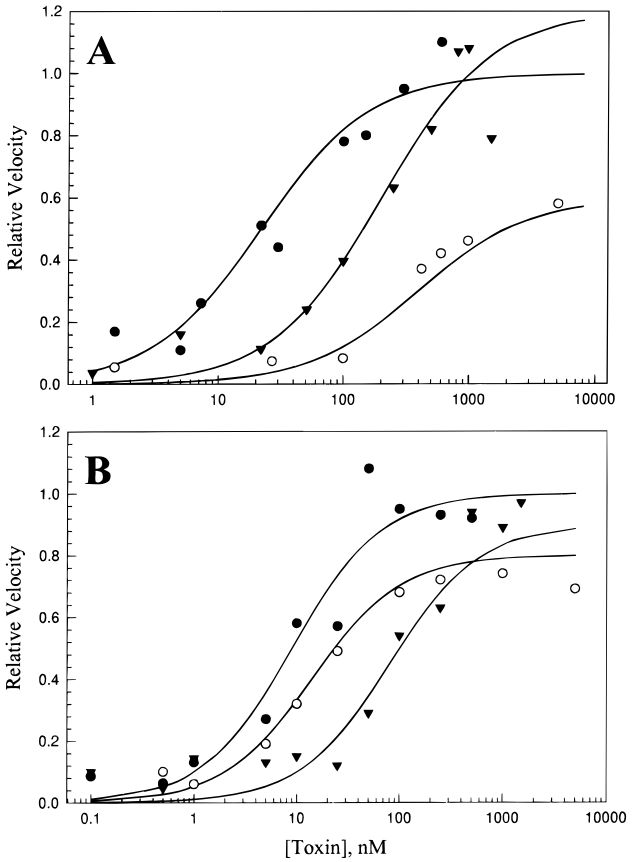

FIGURE 2: Veratridine-dependent sodium uptake in neuronal and cardiac cell lines. The effects of increasing toxin concentration on sodium uptake in N1E-115 (A) and RT4-B (B) cells are shown for ApA (○), ApB (●), and one mutant P13V (▼). Uptake rates were determined as described in Experimental Procedures, corrected for veratridine-stimulated sodium uptake, and normalized to that of wild-type ApB.

Table 2: Functional Characterization of ApB Mutants by Ion Flux

toxin form	V_{max} (normalized to wt)	$K_{0.5}$ (nM)	$K_{0.5(mutant/wt)}$[a]	DI[b]
N1E-115				
wild-type ApB	1.0	22 ± 3	1.0	
P3S	1.1 ± 0.02	104 ± 7	4.7	
P13V	1.2 ± 0.07	202 ± 37	9.2	
N42T	1.2 ± 0.04	24 ± 3	1.1	
I21T	1.3 ± 0.04	49 ± 6	2.2	
F24L	1.0 ± 0.04	105 ± 9	4.8	
R12S/K49Q	1.2 ± 0.05	818 ± 82	37.2	
R12S/P13V/K49Q	1.0 ± 0.02	104 ± 8	4.7	
ApA	0.6 ± 0.02	400 ± 83	18.2	
RT4-B				
wild-type ApB	1.0	9 ± 3	1.0	
P3S	1.0 ± 0.03	17 ± 3	1.9	2.5
P13V	0.9 ± 0.04	81 ± 10	9.0	1.0
N42T	1.2 ± 0.04	31 ± 4	3.4	0.3
I21T	1.1 ± 0.05	26 ± 5	2.9	0.8
F24L	1.1 ± 0.02	22 ± 2	2.4	2.0
R12S/K49Q	0.9 ± 0.02	43 ± 3	4.8	7.8
R12S/P13V/K49Q	1.2 ± 0.03	64 ± 6	7.1	0.7
ApA	0.8 ± 0.04	14 ± 3	1.6	11.4

[a] wt, wild-type. [b] DI, discrimination index = ($K_{0.5(\text{mutant/wt})}$)N1E-115/RT4-B.

Of all the single mutants we examined, only P13V has a major impact on apparent affinity in *both* the cardiac and neuronal assay systems (Figure 3). In the RT4-B line, P13V displays a $K_{0.5}$ of 81 nM, representing a 9-fold decrease in affinity relative to wild-type ApB. None of the other single mutants is changed by more than 3-fold (Table 2). When the P13V is combined with the double mutant R12S/K49Q (Khera et al., 1995), the effects on affinity are non-additive, with the $K_{0.5}$ for the triple mutant (64 nM) being intermediate between those of the double (43 nM) and single (81 nM) mutant parents.

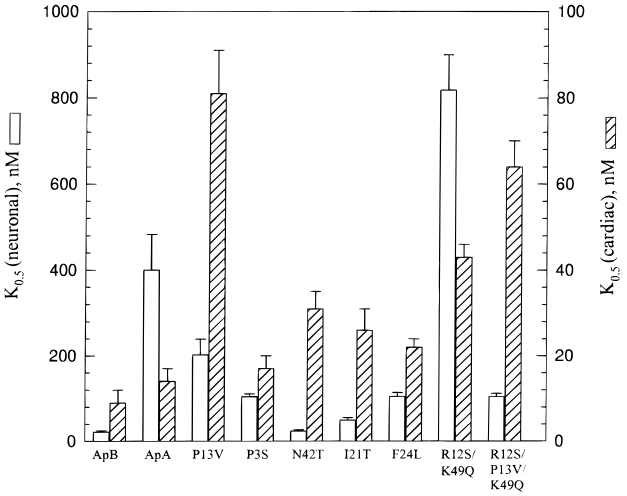

FIGURE 3: Effects of ApB mutations on $K_{0.5}$. Veratridine-dependent sodium uptake rates were used to calculate $K_{0.5}$ values as described in experimental procedures. The data presented in Table 2 are plotted in bar-graph form (including standard error) to facilitate comparison of $K_{0.5}$ values among mutants.

In the N1E-115 line, the effects of the single mutations are analogous in that only the P13V mutant has a significant impact. Its $K_{0.5}$ (202 nM) corresponds to a 10-fold decrease in affinity as compared to wild-type ApB. However, the behavior of the triple mutant toward the neuronal channel differs both qualitatively and quantitatively from that observed with the cardiac isoform. Incorporation of the P13V mutation into the R12S/K49Q context causes an 8-ford *increase* in activity (104 vs 818 nM, Table 2). Indeed, when measured against the neuronal channel, the triple mutant is more active than either of its parentals.

While neither the P3S nor F24L mutants have major effects on apparent affinity (Table 2), it is clear that both mutations yield toxin having an increased ability to discriminate between cardiac and neuronal sodium channels. As seen in Table 2, both mutants display a discrimination index (DI) of about 2, compared to the other single mutants and the triple mutant whose DI's were approximately 1.

Functional Characterization of ApB Mutants by Electrophysiology. We have previously shown that when assayed electrophysiologically, the double mutation R12S/K49Q accounts fully for the difference in affinity between ApA and ApB for neuronal channels and produces a change in affinity to within 2.5-fold of that expected for ApA (Table 3). As in the flux assay, the triple mutant produced a higher affinity toxin for neuronal channels and had a much smaller effect on the affinity for cardiac channels (Table 3). The ordering of toxin preference for cardiac over neuronal isoform is determined primarily by a 17-fold difference in the toxin's off-rate, as compared with a 1.5-fold difference in the calculated on-rate (Figure 4). Overall, the triple mutant toxin shows a 35-fold preference for the cardiac over the neuronal isoform as compared with a 57-fold preference exhibited by the wild-type toxin. However, it is obvious

Table 3: Functional Characterization of ApB Mutants by Electrophysiology

toxin form	k_{on} (10^6 s^{-1} M^{-1})	k_{off} (10^{-3} s^{-1})	K_D (nM)
N1E-115			
ApB[a]	0.93 ± 0.12 ($n = 5$)	4.7 ± 0.1 ($n = 3$)	5.1 ± 0.7
ApA[a]	0.35 ± 0.08 ($n = 7$)	41 ± 1 ($n = 3$)	120 ± 30
R12S/K49Q[a]	0.27 ± 0.08 ($n = 7$)	27 ± 3 ($n = 6$)	100 ± 31
R12S/P13V/K49Q	0.9 ± 0.09 ($n = 8$)	21 ± 8.47 ($n = 8$)	26 ± 11
RT4-B			
ApB[a]	1.4 ± 0.4 ($n = 3$)	0.13 ± 0.01 ($n = 3$)	0.09 ± 0.03
ApA[a]	1.4 ± 0.37 ($n = 3$)	3.5 ± 0.64 ($n = 3$)	2.5 ± 0.9
R12S/K49Q[a]	1.1 ± 0.1 ($n = 11$)	1.0 ± 0.1 ($n = 6$)	0.89 ± 0.11
R12S/P13V/K49Q	1.7 ± 0.27 ($n = 11$)	1.2 ± 0.14 ($n = 5$)	0.72 ± 0.25

[a] Values were taken from Khera et al. (1995).

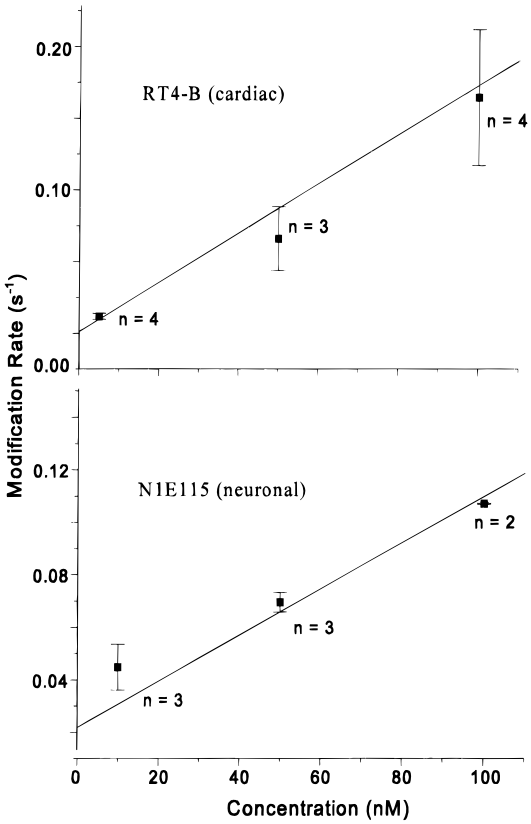

FIGURE 4: Modification rate versus toxin concentration for the ApB triple mutant R12S/P13V/K49Q in cardiac (RT4-B, upper panel) and neuronal (N1E115, lower panel) cell lines. Rate constants were calculated as described in Experimental Procedures. Numbers of cells contributing to the set are indicated. Line is the best linear fit with the intercepts on the ordinate constrained according to the mean off-rates of the toxin, $1.2 \times 10^{-3} \pm 0.1 \times 10^{-3}$ s^{-1} ($n = 5$) for the RT4-B cells and $22 \times 10^{-3} \pm 4.3 \times 10^{-3}$ s^{-1} ($n = 7$) for the N1E-115 cells. $K_D \pm$ SEE values were 0.72 ± 0.25 nM for the RT4-B cells and 26 ± 11 nM for N1E115 cells. Error bars represent standard deviations.

that addition of the P13V mutation to R12S/K49Q fails to account for the K_D difference observed between ApA and the double mutant in the RT4-B cell line. This indicates that contributions from additional sites are involved in defining this toxin's affinity for the cardiac isoform of the sodium channel.

DISCUSSION

Although ApB has the highest affinity of all anemone toxins for the mammalian sodium channel, ApA still retains the greatest capacity to discriminate between the cardiac and neuronal sodium channel isoforms (Schweitz et al., 1981; Kem et al., 1989), with ion flux and electrophysiological assays indicating approximately 30- and 50-fold preferences for the cardiac channel, respectively (Gallagher & Blumenthal, 1994; Khera et al., 1995). Chemical modification studies of sea anemone toxins (Newcomb et al., 1980; Barhanin et al., 1981; Kolkenbrock et al., 1983; Mahnir et al., 1989; Gould et al., 1990) as well as the functionally related α-scorpion toxins (El Ayeb et al., 1986; Kharat et al., 1989) have demonstrated the importance of cationic residues in toxin activity. Likewise, previous work from this laboratory indicates that isoform discrimination can be partially explained by unique cationic residues present at positions 12 and 49 in ApB (Gallagher & Blumenthal, 1994). In that study, three mutants at each of these two unique cationic sites in ApB (Arg-12 and Lys-49) were prepared, in which the native residue was replaced with either a charged, polar, or neutral side chain residue. While mutation of Lys-49 has only minor effects on toxin activity, the nature of the residue at position 12 is more important. Binding affinity in the Arg-12 mutant is reduced by as much as 30-fold, with side chain polarity apparently correlating with affinity. In addition, it is clear that certain substitutions at this position affect the ability of ApB to discriminate between different sodium channel subtypes. In order to ascertain whether the additional uncharged residues unique to ApB play a similar role in regulating toxin affinity, PCR-based site-directed mutagenesis was utilized to convert these remaining residues to those of ApA. All proteins were expressed and purified at comparable levels, indicating that none of these residues serve as key structural determinants in the toxin. This is reinforced by their similar secondary structures (approximately 55% β-sheet) and stability to thermal denaturation.

Upon examination of the data summarized in Table 2, it is obvious that the P13V mutation has the largest effect, causing a 10-fold loss of activity in both cell lines. Based on its proximity to Arg-14, which is conserved in all known anemone toxins (Norton, 1991), and Arg-12, whose importance we have already demonstrated, this is most likely due to its impact on backbone conformation within the Arg-14 loop, a flexible region between residues 9 and 18. In contrast, an analogous proline replacement, P3S, causes little change in overall activity. However, the 5-fold loss of affinity seen in the neuronal line for this mutant is more than twice that observed in the cardiac cell line, suggesting a possible role for Pro-3 in channel isoform discrimination. The F24L mutation, in a loop region connecting two β-strands, also displays a similar profile, suggesting an analogous role in selectivity. The prominent failure of all

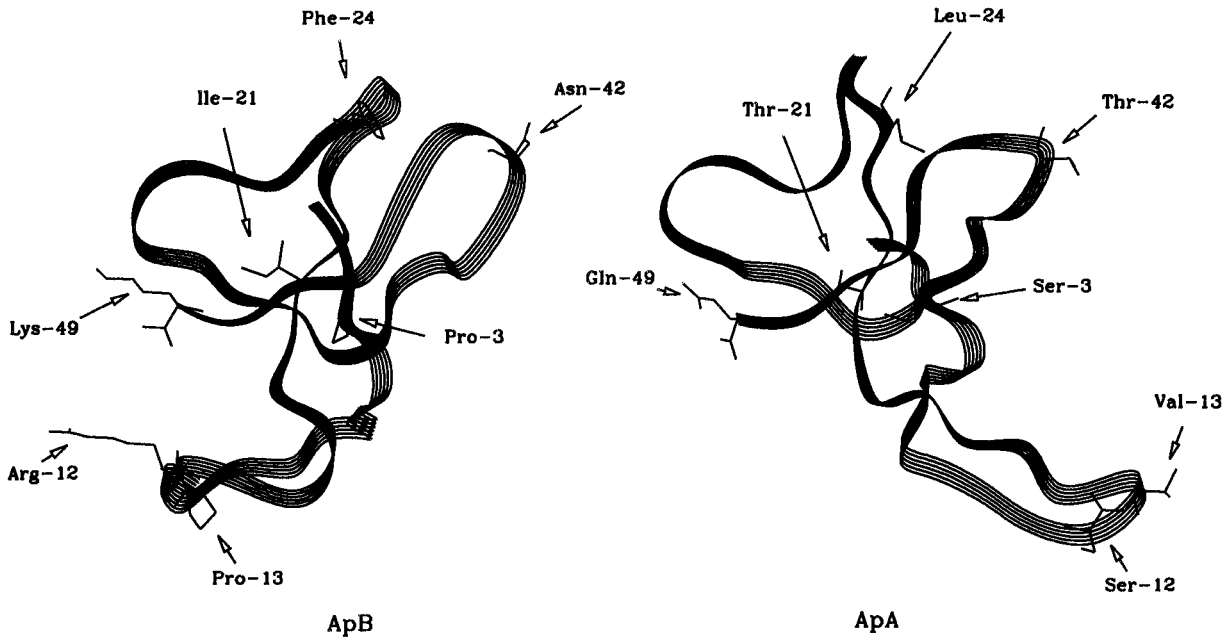

FIGURE 5: Distribution of mutagenized sites in the three-dimensional structures of ApB (left) and ApA (right). Backbones of each molecule are represented in ribbon format, and the positions targeted are annotated for each protein. The coordinates for ApA were taken from Pallaghy et al. (1995) as deposited in the Protein Database (pdb1ahl.ent), while the structure depicted for ApB is based on the model developed in this laboratory (Khera et al., 1995). Note the close similarity between the backbone structures of the two toxins, with the exception of the orientation of the Arg-14 loop described in the text.

the mutants tested thus far to alter V_{max} indicates that the ability of these toxins to stabilize the open conformation of the channel is unaltered.

During the course of this study, the solution structures of both ApA (Pallaghy et al., 1995) and ApB (Monks et al., 1995) were published, and the coordinates of both have recently been made available in the Brookhaven database. The core structures of both polypeptides consist of a four-stranded, antiparallel β-sheet (residues 2−4, 20−23, 34−37, and 45−48) and include three β-turns (residues 6−9, 25−28, and 30−33). Three loops connect the β-strands, with the Arg-14 loop (residues 9−18) being both the longest and least well defined (Monks et al., 1995). Aside from the I21T and P3S mutations, all of the mutations in this study occur in loop regions having little defined secondary structure. However, at least two residues known to be essential for ApB binding, Arg-12 and Leu-18 (Gallagher & Blumenthal, 1994; Dias-Kadambi et al., 1996a), are found within the first loop.

The solution structures of both ApB and ApA also predict clustering of charged residues believed to be involved in toxin binding, in agreement with molecular modeling studies of ApB (Khera et al., 1995). Figure 5 compares the backbone conformations of Norton's average structure of ApA to our ApB model, demonstrating that with the exception of the Arg-14 loop (residues 9−18), the two toxins are highly related. While the orientation of the Arg-14 loop in the structure of ApA and our model of ApB differ, examination of the structure of ApB (Monks et. al., 1995) confirms that its Arg-14 loop is oriented approximately as predicted by the model. Thus the model represents a reasonable framework in which to interpret the results of mutagenesis studies. Figure 5 further depicts that all of the sites characterized in this study as not greatly affecting toxin affinity are remote from both the Arg-14 loop and the cationic cluster encompassing Arg-12, Arg-14, and Lys-49. The combined importance of this region is also underscored by recent mutagenesis studies in which Leu-18 and Trp-33 were targeted on the basis of their modeled proximity to cationic residues of the loop (Dias-Kadambi et al., 1996a,b). Mutagenesis of Leu-18 to valine causes several hundred-fold losses in affinity on either isoform of the sodium channel. In our study, mutation of the nearby Ile-21 has only a minimal effect on activity. When taken together, these results locate a boundary between Leu-18 and Ile-21 for the binding epitope in this region of the molecule.

The activity toward neuronal channels of the double mutant R12S/K49Q, in which the two unique cationic residues in ApB are simultaneously mutated to those found in ApA, is reduced to a much greater extent than for cardiac channels, wherein $K_{0.5}$ values are quite similar to those of ApA (Khera et al., 1995). Therefore, we reasoned that combining this double mutant with the P13V substitution might produce a toxin with even weaker binding to the neuronal sodium channel and thus better suited to channel isoform discrimination. However, the new triple mutant R12S/P13V/K49Q is no longer able to discriminate between sodium channel isoforms and even displays an *enhanced* affinity for the neuronal isoform when compared to either the single mutant P13V (2-fold) or the double mutant R12S/K49Q (8-fold). This result has been confirmed by electrophysiological analysis and may arise from removal of the highly constrained proline residue, allowing the toxin more degrees of freedom to interact favorably with target sequences of the neuronal sodium channel.

All available data highlight the importance to activity of at least four residues within the Arg-14 loop in both ApA and ApB (Pallaghy et al., 1995; Monks et al., 1995; Khera et al., 1995; Gallagher & Blumenthal, 1994; Dias-Kadambi et al., 1996a). It is our belief that the increased activity of ApB, as well as the discriminatory ability inherent in ApA, is partially due to residues unique to this region. Of those loop sites targeted by our laboratory, the P13V replacement has the greatest ability to alter both the conformation and

flexibility. Thus, Pro-13 has the ability to affect function in one of two ways: either through direct contacts with the binding site or via conformational effects. We believe it is unlikely that the effects of P13V are due to direct contact, since both proline and valine are fairly hydrophobic side chains. More likely, the presence of Pro-13 would tend to restrict the number of conformations available to the Arg-14 loop. In this scenario, ApA is less active on neuronal channels than ApB because the absence of Pro-13 allows other residues in the Arg-14 loop to assume a conformation less favorable to high affinity binding. Further evidence for the role of Pro-13 in high-affinity binding due to its effects on conformation could come through the analysis of additional loop mutants, with the goal of creating a more conformationally restricted toxin.

In summary, the new insights into anemone toxin binding and discrimination gained in this and earlier studies have highlighted several key ApB sites essential for its cardiotonic activity. Moreover, the localization of several of these residues within the conformationally flexible Arg-14 loop underscores the importance of obtaining high-resolution structural information on this region of anemone toxins. Since the potential for these polypeptides as cardiotonic agents clearly exists, such information will aid in the design of templates for the directed synthesis of new cardiotonic drugs in the future.

REFERENCES

Alsen, C. (1983) *Federation Proc. 42*, 101−108.

Barhanin, J., Hugues, M., Schweitz, H., Vincent, J.-P., & Lazdunski, M. (1981) *J. Biol. Chem. 256*, 5764−5769.

Bradford, M. M. (1976) *Anal. Biochem. 72*, 248−254.

Catterall, W. A. (1980) *Annu. Rev. Pharmacol. Toxicol. 20*, 15−43.

Catterall, W. A. (1984) S*cience 223*, 653−661.

Catterall, W. A. (1995) *Annu. Rev. Biochem. 64*, 493−531.

Catterall, W. A., & Beress, L. (1978) *J. Biol. Chem. 253*, 7393−7396.

Cleland, W. W. (1979) *Methods Enzymol. 63*, 103−138.

Dias-Kadambi, B. L., Drum, C. L., Hanck, D. A., & Blumenthal, K. M. (1996a) *J. Biol. Chem. 271*, 9422−9428.

Dias-Kadambi, B. L., Comb, K. A., Drum, C. L., Hanck, D. A. & Blumenthal, K. M. (1996b) *J. Biol. Chem. 271*, 23828−23835.

Donahue, L. M., Schaller, K., & Sueoka, N. (1991) *Dev. Biol. 147*, 415−424.

El Ayeb, M., Darbon, H., Bahraoui, E. M., Vargas, O., & Rochat, H. (1986) *Eur. J. Biochem. 155*, 289−294.

Fozzard, H. A., & Hanck, D. A. (1996) *Physiol. Rev. 76*, 887−926.

Gallagher, M. J., & Blumenthal, K. M. (1992) *J. Biol. Chem. 267*, 13958−13963.

Gallagher, M. J., & Blumenthal, K. M. (1994) *J. Biol. Chem. 269*, 254−259.

Gould, A. R., Mabbutt B. C., & Norton, R. S. (1990) *Eur. J. Biochem. 189*, 145−153.

Gross, G. J., Warltier, D. C., Hardman, H. F., & Shibata, S. (1985) *Eur. J. Pharm. 110*, 271−276.

Hanck, D. A., & Sheets, M. F. (1995) *J. Gen. Physiol. 106*, 601−16.

Hirsch, J. K., & Quandt, F. N. (1996) *Brain Res. 706*, 343−346.

Kem, W. R., Parten, B., Pennington, M. W., Price, D., & Dunn, B. M. (1989) *Biochemistry 28*, 3483−3489.

Kharat, R., Darbon, H., Rochat, H., & Granier, C. (1989) *Eur. J. Biochem. 181*, 381−390.

Khera, P. K., & Blumenthal, K. M. (1994) *J. Biol. Chem. 269*, 921−925.

Khera, P. K., Benzinger, R., Lipkind, G., Drum, C. L., Hanck, D. A., & Blumenthal, K. M. (1995) *Biochemistry 34*, 8533−8541.

Kolkenbrock, H. J., Alsen, C., Asmus, R., Beress, L., & Tschesche, H. (1983) *Proc. Eur. Symp. Animal, Plant, Microb. Toxins, 5th* (Mebs, D., & Habermehl, G., Eds.) 72.

Mahnir, V. M., Kozlovskaya, E. P., & Elyakov, G. B. (1989) *Toxicon 27*, 1075−1084.

Monks, S. A., Pallaghy, P. K., Scanlon, M. J., & Norton, R. S. (1995) *Structure 3*, 791−803.

Narahashi, T., & Herman, M. D. (1992) *Methods Enzymol. 207*, 620−643.

Newcomb, R., Yasunobu, K. T., Seriguchi, D., & Norton, T. R. (1980) *Frontiers in Protein Chemistry* (Liu, D. T., Mamiya, G., & Yasunobu, K. T., Eds.) pp 539−550, Elsevier-North Holland, New York.

Noda, M., Shimizu, S., Tanabe, T., Takai, T., Kayano, T., Ikeda, T., Takahashi, T., Nakayama, H., Kanaoka, Y., Minamino, N., Kangawa, K., Matsuo, H., Raftery, M., Hirose, T., Inayama, S., Hayashida, H., Miyata, T., & Numa, S. (1984) *Nature 312*, 121−127.

Norton, R. S. (1991) *Toxicon 29*, 1051−1084.

Pallaghy, P. K., Scanlon, M. J., Monks, S. A., & Norton, R. S. (1995) *Biochemistry 34*, 3782−3794.

Ravens, U. (1976) *Naunyn−Schmiedeberg's Arch. Pharmacol. 295*, 55.

Ray, R., Morrow, C. S., & Catterall, W. A. (1978) *J. Biol. Chem. 253*, 7307−7313.

Schweitz, H., Vincent, J.-P., Barhanin, J., Frelin, C., Linden, G., Hugues, M., & Lazdunski, M. (1981) *Biochemistry 20*, 5245−5252.

Shibata, S., Norton, T. R., Izumi, T., Matsuo, T., & Katsuki, S. (1976) *J. Pharmacol. Exp. Ther. 199*, 298−309.

Tejedor, F., & Catterall, W. A. (1988) *Proc. Natl. Acad. Sci. U.S.A. 85*, 8742−8746.

Torda, A. E., Mabbutt, B. C., van Gunseren, W. F., & Norton, R. S. (1988) *FEBS Lett. 239*, 266−270.

Zeng D., Kyle, J. W., Martin, R. L., Ambler, K. S., & Hanck, D. A. (1996) *Am. J. Physiol. 270* (*Cell Physiol. 39*), C1522−C1531.

BI961584D